UNIVERSITY OF BRISTOL

Peer reviewed version

Link to published version (if available):
10.1088/0964-1726/24/11/115014

Link to publication record in Explore Bristol Research
PDF-document

Design of an embedded sensor, for improved structural performance.

James S Chilles[1], Anthony Croxford[2], Ian P Bond[1]

[1] Advanced Composites Centre for Innovation and Science, University of Bristol, Queen's Building, Bristol BS8 1TR, UK
[2] Department of Mechanical Engineering, University of Bristol, Queen's Building, Bristol, BS8 1UB, UK

E-mail: jc9191@bristol.ac.uk

October 2015

Abstract.
Low velocity impact damage to composite laminates can result in a complicated network of matrix cracks and delaminations beneath the laminates surface, which are extremely difficult to detect by visual inspection. Current non-destructive evaluation (NDE) techniques such as ultrasonic C-Scan and X-Ray imaging create significant downtime, which leads to costly inspection programmes. Embedded sensors offer the potential to increase the automation of inspection, and decrease the downtime when compared with current NDE practices. However, for such systems to be practical, sensors must be integrated within composite structures without producing unacceptable loss of structural performance. This paper identifies techniques for embedding slim sensors with comparatively large in-plane dimensions inside composite materials. Interlaminar shear strength tests were used to identify an encapsulating layer for the sensors. Flexural strength testing was carried out on laminates containing sensors embedded towards the compressive surface of flexural specimens. The experimental study was complemented with finite element analysis, which identified the load paths within different embedment configurations and aided with the interpretation of the experimental results. The results show that with careful selection of sensor materials, geometry, embedding location and embedment technique, sensors can be integrated within composite structures without producing any significant reduction of mechanical performance.

Keywords: Embedded sensors, Composite materials, Structural integrity

1. Introduction

The use of fibre reinforced plastics within aerospace structures has increased dramatically in the last decade, due to the excellent specific stiffness and strength that these materials possess. However, the potential loss of structural integrity due to low velocity impacts, such as the dropping of tools or poor handling of parts is cause

for concern. When impacted a complex network of matrix cracks and delaminations may form deep within the structure, which if left untreated can lead to catastrophic failure [1]. To further compound the problem, low velocity impact damage is extremely difficult to detect by visual inspection [2]. Current non-destructive evaluation (NDE) techniques such as X-Ray or ultrasonic C-Scan imaging require expensive equipment, skilled operators and the part to be taken out of service. This creates inconvenient and expensive inspection programmes. A potential alternative is to permanently attach or embed sensor arrays (within structures), that are capable of monitoring and assessing the development of damage; such systems could automate the inspection of composite structures, which would lead to increased reliability, reduced operational costs and decreased downtime when compared with conventional NDE methods.

The clear potential of permanently attached sensor networks has led to significant work being carried out within the field of structural health monitoring. However, a relatively small amount of this work focuses on integrating the sensors within structures, with the majority focusing on the design of sensor components or the development of new signal processing techniques. Mall et al [3, 4] investigated the impact on structural performance of embedding wired piezoelectric sensors within quasi-isotropic carbon fibre specimens, under both monotonic and fatigue tensile loading conditions. It was found that when embedding sensors between plies that are not aligned with the loading direction, the presence of the embedded piezoelectric sensors had no effect on structural performance. Various researchers [5, 6, 7, 8] have evaluated the influence of different embedment configurations on the tensile strength of unidirectional composite specimens. The experimental results show that by dispersing the discontinuities at ply cuts between continuous plies, both the initiation and ultimate failure loads can be increased when compared with inclusions embedded by cutting all of the plies at one location. The results highlight the importance of embedment technique selection, but do not evaluate the influence of laminate stacking sequence. Ghezzo et al [9] investigated the effect of embedding rectangular inclusions on the tensile strength of unidirectional glass fibre laminates. The specimens failed by debonding along the interface of the embedded inclusion and the surrounding composite. The accompanying numerical analysis [10] indicated that there existed significant interlaminar stress concentrations at the sensor-composite interface. The results show the importance of the embedded item's geometry, and the bond strength between an inclusion and the surrounding composite material.

Whilst the previously mentioned works highlight some of the issues faced when embedding sensors within composite materials, in each case the chosen loading regime was tensile. The critical load case when embedding within composites is compressive, as a greater reliance is placed on the matrix and embedded item to carry load [11, 12, 13]. This is supported by the experimental work of Shivakumar and Emmanwori [12], which characterised the effects of embedding optical fibres within unidirectional carbon fibre laminates. It was found that the compressive strength reduced by 40%, compared with the smaller 10% reduction found to occur when loading the same laminate in tension. The structural integrity of the SMART layer [14, 15], a network of wired piezoelectric

transducers contained within a dielectric layer, was assessed using compression testing. The compressive strength of quasi-isotropic carbon fibre laminates was compared to those containing an embedded SMART layer at the midplane, and no reduction in compressive strength was found. However, the tested laminate layup separated the embedded SMART layer and plies aligned with the compressive load with six off axis plies. This represents an optimistic structural configuration, as the fibre waviness induced by the presence of an embedded inclusion decreases with increasing distance from the inclusion. To accurately assess the impact on structural integrity, the distance between load bearing plies and the embedded feature should be varied to include more conservative laminate configurations.

This paper evaluates the implications of embedding slim sensors with comparatively large in-plane dimensions inside composite materials. Specifically, inductively coupled piezoelectric sensors as described in the work of Zhong et al [16, 17]. Each sensor consists of a piezoelectric transducer connected to an inductance coil. When a pair of coaxial transmit and receive coils are held over the sensor, power is wirelessly transmitted via inductive coupling to the otherwise passive sensor. Once activated, the piezoelectric disk generates ultrasonic waves, which are used to interrogate the structure. The inductive coupling between the sensor and external probe removes the need for wired connections within the structure. This makes the inductively coupled system lighter than wired embedded sensing networks, and eliminates the potential for failure initiation at the connecting wires, as was observed in the experimental work of Tang et al [18]. The inductively coupled sensors have a total diameter of 50 mm and maximum thickness of 0.45 mm. Whilst the sensors are large in comparison to other embedded inclusions such as self healing vascules and fibre optic sensors [11, 12, 13], they possess the advantage of being remote devices which use ultrasonic waves to interact with damage, this allows the sensors to be embedded in relatively unloaded through-thickness locations and structural positions. The aim of this study was to identify the optimum strategy for embedding thin remote sensing devices, with comparatively large in-plane dimensions inside composite materials. The embedding strategy includes decisions such as the selection of the encapsulating layer, sensor geometry, embedding technique and through-thickness embedding location within the host laminate. An encapsulating layer for the sensor's was identified using interlaminar shear strength testing. Four-point bend flexural strength testing was used to characterise the effect of embedding sensors on structural performance. To evaluate the effect of sensor integration under the critical compressive load case, sensors were embedded towards the compressive surface of the flexural specimens. To aid with the analysis of the flexural strength testing, plane strain finite element models were constructed according to the geometry of specimen cross sections, which were identified using optical microscopy. The models identified the load paths for each embedding technique, and aided with identification of both the failure initiation sites and modes observed in the flexural strength testing. This study focuses on embedding inductively coupled piezoelectric sensors, however the results are applicable to any high aspect ratio remote sensor embedded in a composite material.

2. Experimental testing

This section contains descriptions of the experimental approach and results of the interlaminar shear and flexural strength testing. Polyimide has high mechanical toughness and is an electrical insulator, which makes it a suitable material to encapsulate sensors embedded in composites reinforced with conductive carbon fibres, however polyimide must be surface treated to ensure it bonds with the surrounding composite material [19]. Interlaminar shear strength testing was used to identify a surface treated polyimide layer capable of forming a strong mechanical bond with a composite matrix.

To investigate the effect of sensor integration on compressive behaviour, and identify embedment configurations that allow sensors to be integrated without reducing structural performance, four-point bend flexural strength testing was selected. Flexural strength testing was chosen rather than axial compression testing, due to the large diameter of the embedded sensors exceeding the gauge length available in a standard axial compression test. Four-point bend flexural strength testing allowed the appropriate span to thickness and loading span to support span ratios to be chosen, such that the sensors were embedded between the two loading rollers, in a region subjected to a constant bending moment. To evaluate the compressive behaviour, the sensors were embedded towards the compressive surface of the flexural specimens.

2.1. Specimen manufacture

All of the specimens were manufactured from a unidirectional glass fibre epoxy composite prepreg system (Hexcel, E-Glass 913 prepreg). In all cases the laminates were manufactured using the hand layup process. The assembled stacking sequences were then cured inside an autoclave at 125 °C under 7 bar of pressure for 1 hour. The cure cycle of specimens greater than 3 mm thick included a 30 minute dwell period at 95 °C. All the specimens were cut from larger plates using a water cooled diamond saw. The cut specimens were then polished to aid with the optical microscopy of their cross sections.

2.1.1. Interlaminar shear strength specimens

Interlaminar shear strength specimens were manufactured in accordance with BS EN 2563:1997 [20]. Each specimen was unidirectional with a layup of $[0°]_{14}$. The beams were cut to a length of 20 mm, and width of 10 mm. Within this data set there were a total of four experimental groups (Table 1). Two polyimide layers supplied by different manufacturers (groups A and B, Table 1) were soaked in Diethylenetriamine for 24 hours to improve the adhesion with the epoxy matrix, as advised in the work of Yasaee [19]. Group C (Table 1) contained a commercially available product (Pyralux LF bond ply, Dupont); a polyimide layer coated on either side with B-staged acrylic adhesive. The polyimide layers in groups A,B and C were all embedded at the midplane of the interlaminar shear specimens.

Table 1. Interlaminar shear strength testing experimental groups.

Experimental Group	Polyimide film	Surface treatment	Thickness of layer (mm)	Total thickness (mm)
Control	N/A	N/A	0	2.06 ± 0.09
A	Upilex 50RN	Diethylenetriamine	0.05	2.19 ± 0.06
B	Kapton film	Diethylenetriamine	0.10	2.26 ± 0.07
C	Bond ply	Acrylic adhesive	0.075	2.14 ± 0.07

2.1.2. Four-point bend flexural strength specimens

The four-point bend flexural strength specimens were manufactured to meet ASTM-D6272 -10 [21]. Beams were cut to a length of 160 mm, and width of 20 mm. The 50 mm diameter of the sensors, exceeded the width of the flexural specimens (shown in Figure 1a). Therefore, representative two dimensional planar sections were embedded towards the compressive surface of the flexural specimens. The use of planar sensor sections covering the full width of the specimens made the flexural testing conservative; when embedded in a real structure the sensors will only cover a small proportion of the host structure's area. Figure 1a shows a sensor and its cross section, alongside a four-point bend test specimen containing a planar sensor section.

Two methods were used to embed the sensor sections within flexural specimens. The first embedment method placed sensor sections into the laminates stacking sequence, without altering their geometry. This method, termed the forming method, maintained continuous fibres but introduced fibre waviness into the adjacent plies (as shown in Figure 2a). The second embedding technique applied to embed sensor sections altered the sensors geometry, and cut three of the flexural specimens plies. Prior to embedding, resin film (Hexcel, 913 film) was laid onto the inductance coil, to compensate for the
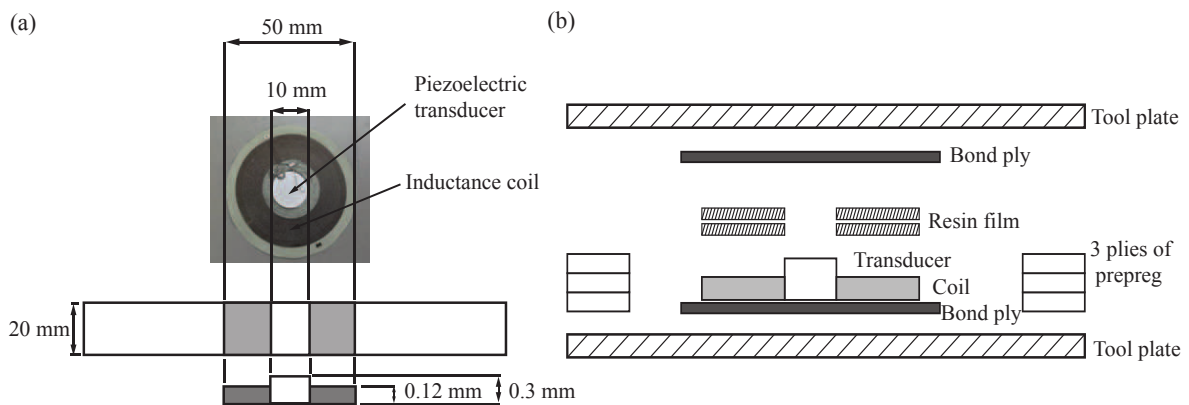

Figure 1. a) Inductively coupled sensor, and diagrams of the representative section embedded into the flexural specimens. b) Assembly used to manufacture rectangular sensor sections.

difference in thickness between the coil and transducer. The assembly was clamped between two steel plates and partially cured at 100°C for 1 hour, three plies of prepreg were used as the mould spacing (as shown in Figure 1b). Sensor sections with a rectangular cross section were then embedded into the removed region of prepreg. This embedding technique termed, the cut ply method, minimised the fibre misalignment introduced into the adjacent plies, but cut three of the flexural specimens plies (shown in Figure 2b).

Figure 2. a) Forming embedding technique. b) Cut ply embedding method.

2.2. Experimental Method

2.2.1. Interlaminar shear strength testing

The specimens were loaded in a three point bend configuration using three rollers, each of radius 3 mm. The applied loading rate was 1 mm/min as advised by the standard [20]. The test geometry is shown in Figure 3a. The experimental groups are summarised in Table 1. Each group consisted of five replicates.
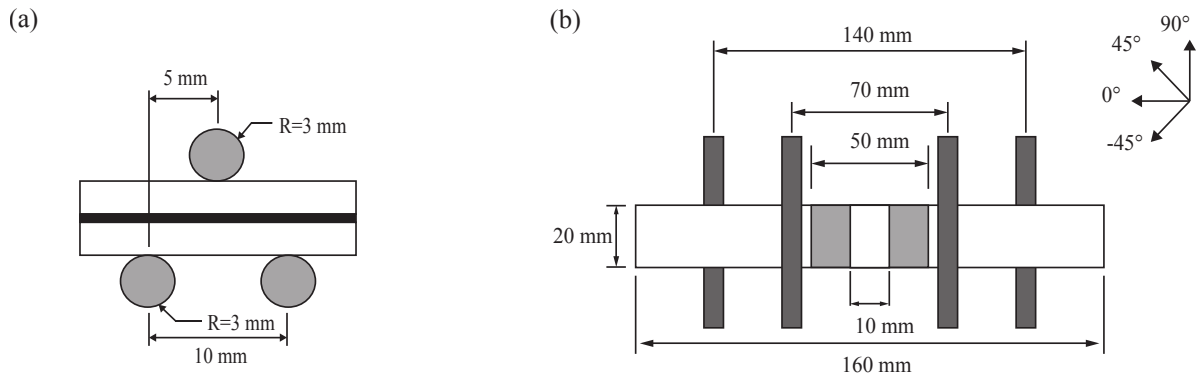

Figure 3. a) Interlaminar shear strength test geometry. b) Four-point bend flexural strength test geometry.

2.2.2. Four-point bend testing

Four-point bend flexural strength testing according to ASTM- D6272-10 was chosen to characterise the flexural strength of laminates containing sensors embedded towards the compressive surface. The selected ratio of support span to load span was 2:1 and a loading rate of 5 mm/min was applied to all specimens. The test geometry is displayed in Figure 3b. The flexural strength testing contained nine specimen groups (Table 2). The

embedding locations (Figure 4a), embedding techniques and internal components were all varied to assess their influence on the structural performance of a highly orthotropic laminate (Laminate A, Figure 4a). The laminates thickness of 4.38 mm $\pm$ 0.13 (30 plies), resulted in the flexural testing being carried out with a span to thickness ratio of 32:1. Sensors were then embedded into a second laminate with a quasi-isotropic layup widely found in industrial applications (Laminate B, Figure 4b). This allowed the effectiveness of the identified embedding strategies to be evaluated in an industrially relevant composite structure. Laminate B was 4.96 mm $\pm$ 0.04 thick (32 plies), reducing the span to thickness ratio to 28:1.
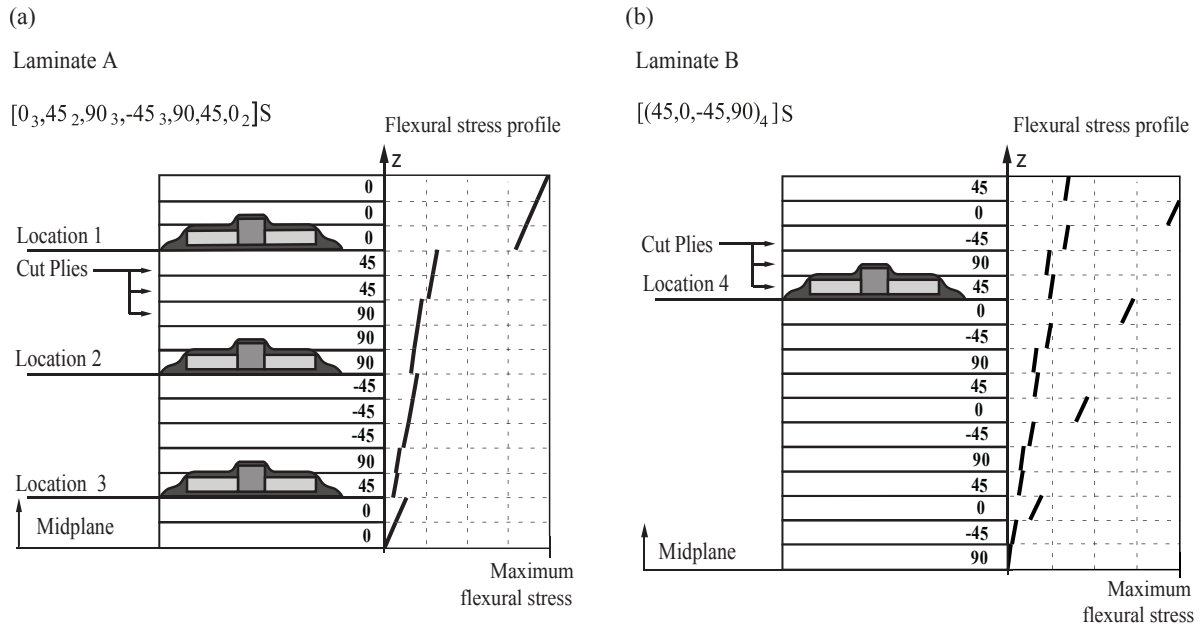

Figure 4. a) Stacking sequence, embedding locations and flexural stress profile of Laminate A. b) Stacking sequence, embedding locations and flexural stress profile of Laminate B. The stress profiles were calculated using classical laminate theory [22].

Table 2. Four-point bend flexural strength specimens.

Group	Laminate layup	Embedding method	Embedding location	Transducer material	Thickness (mm)
Control	A	N/A	N/A	N/A	4.38 $\pm$ 0.13
A	A	Formed	3	Steel	4.72 $\pm$ 0.12
B	A	Formed	2	Steel	4.75 $\pm$ 0.14
C	A	Formed	1	Steel	4.78 $\pm$ 0.14
D	A	Formed	1	Carbon	4.80 $\pm$ 0.11
E	A	Cut ply	1	Carbon	4.35 $\pm$ 0.12
Control	B	N/A	N/A	N/A	4.96 $\pm$ 0.04
F	B	Cut ply	4	Carbon	4.89 $\pm$ 0.14
G	B	Formed	4	Carbon	5.37 $\pm$ 0.17

2.3. Microscopic characterisation of embedded sensors

The polished flexural strength specimen cross sections (Figures 5a and 5b) were analysed using optical microscopy (Olympus SZX16 microscope with Colorview camera). Geometrical parameters were measured using image processing software (ImageJ), and the recorded values averaged across a sample of five specimens. The averaged parameters were used to construct idealised two dimensional models of each embedding technique (Figure 5c and 5d).

2.4. Experimental results and discussion

2.4.1. Interlaminar shear strength results

Table 3 displays the interlaminar shear strength data for the experimental groups described in Table 1. The control specimens failed in an interlaminar shear failure mode; a delamination propagated along the midplane of the specimen. The introduction of the films embedded in groups A and B (Table 1) reduced the interlaminar shear strength (Table 3). In each case a crack was seen to propagate along the interface between the composite and embedded film. The interlaminar shear strength of experimental group C (Table 3) was slightly lower than the control samples, however, the shear failure occurred between the plies of the composite. The interface between the film and composite remained undamaged, therefore, the film embedded in experimental group C (Pyralux LF bond ply, Dupont) was selected as the sensor's encapsulating layer for the subsequent flexural strength testing.

Table 3. Interlaminar shear strength results.

Experimental group	Interlaminar shear strength (MPa)	Percentage strength
Control	106.3 ± 5.6	100
A	69.1 ± 4.9	65
B	72.9 ± 5.9	69
C	97.3 ± 3.0	92

2.4.2. Characterisation of embedded sensor geometry

The geometrical parameters in Table 4, measured from the optical microscopy of specimen cross sections (Figures 5a and 5b), were used to construct the idealised geometries of laminates containing sensors embedded using the cut ply and forming techniques (Figures 5c and 5d). Table 4 shows the fibre misalignment angles at each ramped change in sensor thickness created by embedding a formed sensor (labelled regions A,B and C, Figure 5a), and the dimensions of each component within both sensor types. The decrease of fibre misalignment angle with increasing distance from sensors embedded using the forming technique (Table 4), indicates that formed sensors should not be embedded directly beneath major load bearing plies.
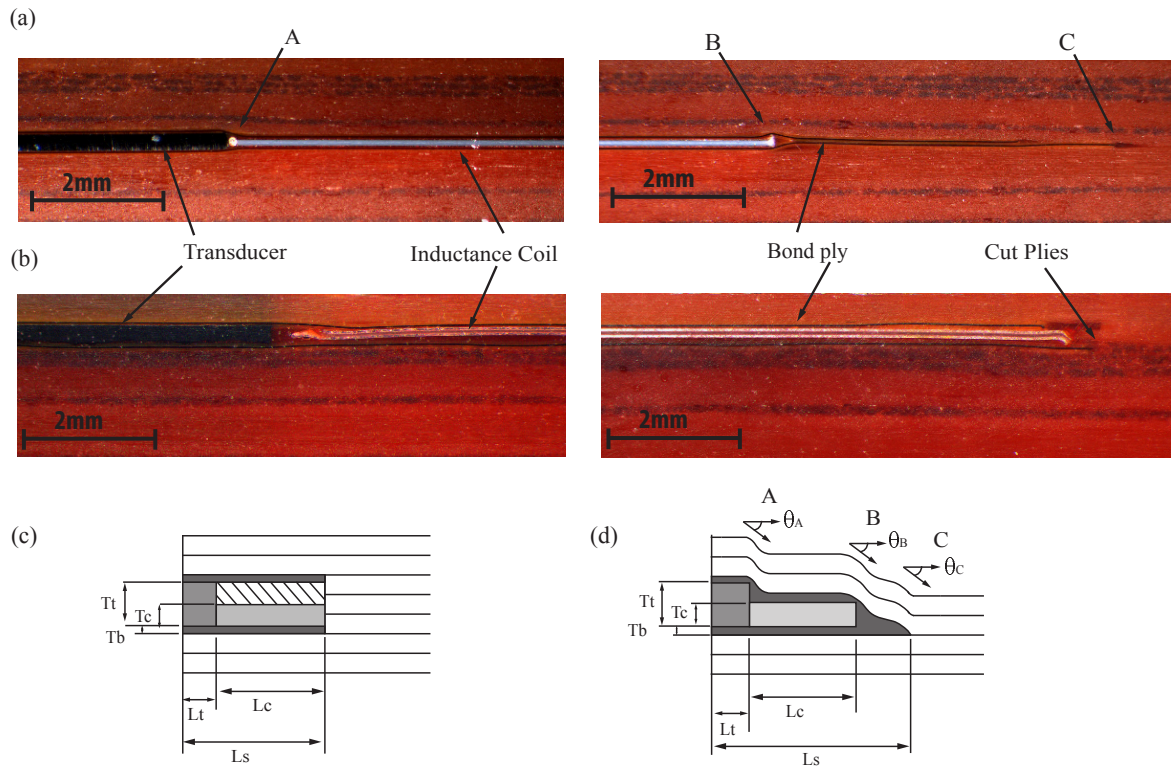
Figure 5. a) Sensor embedded using the forming technique. b) Sensor embedded using the cut ply method. c) Idealised cut ply sensor geometry. d) Idealised formed sensor geometry.

Table 4. Fibre misalignment created by embedding a formed sensor, and dimensions of the sensor components, measured in millimeters.

	Misalignment Angle at each interface (°)		
Distance above	A	B	C
embedded sensor	θ_A	θ_B	θ_C
0	4.22±0.59	2.99 ± 0.79	2.28 ± 0.26
1 ply	3.42±0.63	2.23 ± 0.41	1.74 ± 0.15
5 plies	1.82±0.55	1.47 ± 0.13	1.24 ± 0.09
10 plies	0.79±0.30	0.72 ± 0.16	0.78 ± 0.20

Embedding method	L_t	L_c	L_s	T_t	T_c	T_b
Formed	7.5	17.5	30.0	0.3	0.12	0.075
Cut Ply	7.5	17.5	25.0	0.3	0.12	0.075

2.4.3. Four-point bend flexural strength results

Table 5 describes the flexural strength results obtained from the four-point bend testing of the experimental groups shown in Table 2. The control specimens for layups A and B (Figures 4a and 4b) failed in a tensile failure mode (Table 5). The gradual growth

Table 5. Four-point bend flexural strength results.

Group	Laminate layup	Flexural strength (MPa)	Failure mode	
Control	A	751 ± 57		Fibre failure at the tensile surface.
A	A	731 ± 71		Fibre failure at the tensile surface.
B	A	729 ± 67		Fibre failure at the tensile surface.
C	A	395 ± 81		Disbonding between transducer and bond ply, followed by buckling.
D	A	709 ± 29		Compression failure directly above the transducer inductance coil interface.
E	A	764 ± 62		Fibre failure at the tensile surface.
Control	B	698 ± 29		Fibre failure at the tensile surface.
F	B	699 ± 31		Fibre failure at the tensile surface.
G	B	671 ± 32		Fibre failure at the tensile surface.

(a)

(b)

(c)
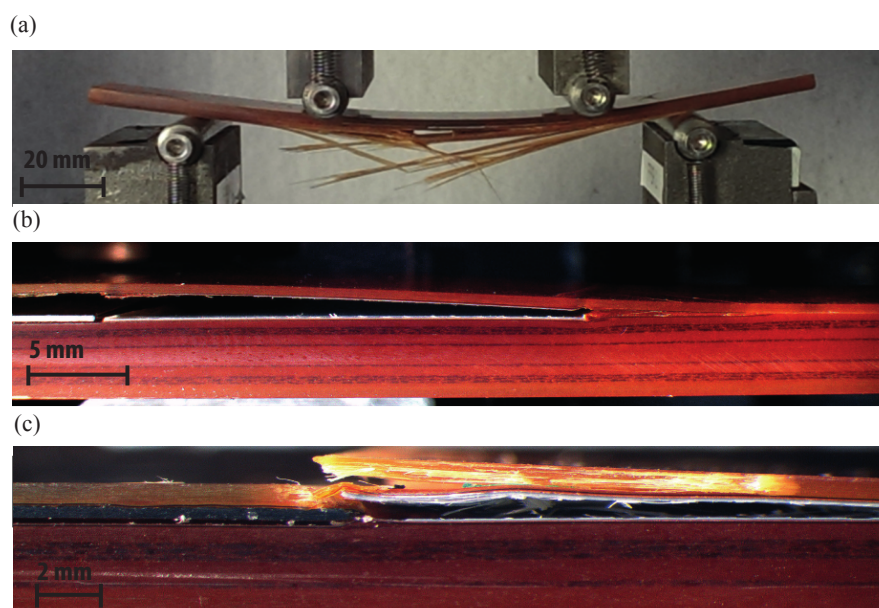
Figure 6. a) Tensile failure mode (groups A,B,E,F,G and control specimens). b) Buckling failure (group C). c) Compression at the transducer inductance coil interface (group D).

of delaminations led to the breaking of the fibres on the tensile surface of the flexural specimens (Figure 6a). This failure mode is in agreement with other flexural strength tests carried out on glass fibre epoxy laminates [23, 24].

The tensile failure modes of experimental groups A and B (Table 5), show that when

a formed sensor is embedded in an unloaded region of a laminate (Table 2 and Figure 4a) the sensor does not cause the laminate to fail prematurely. The slight reduction in flexural strength is due to the thickness increase (Table 2) caused by integration of a formed sensor affecting the flexural strength calculations. The failure loads of experimental groups C and D, show the importance of the internal bond strengths when embedding formed sensors in highly loaded regions (Table 2 and Figure 4a). Weak internal bonds within the sensor (Table 5, group C), resulted in the sensor behaving in the same way as near surface delaminations, and initiating buckling (Figure 6b) under compressive load [25, 26]. The flexural specimens containing sensors with strongly bonded transducers (Table 5, group D) failed at a significantly higher failure load. Due to the close proximity of the compressive failure associated with the sensor to the tensile failure load of the flexural specimens, the specimens did not fail in a consistent failure mode (2 specimens failed in compressive, and 3 failed in tensile failure mode). Table 5 (group D) and Figure 6c show the compressive failure associated with the embedded sensor. The tensile failure of experimental group E (Table 5) demonstrates that cut ply sensors can be integrated into composite structures without initiating failure, providing the major load bearing plies are not cut to accommodate the sensor (Figure 4a).

The flexural strength testing of experimental groups F and G evaluated the ability to integrate sensors within a quasi-isotropic layup widely used in industrial applications (Figures 4b). The plies cut to integrate the sensor in specimen group F (Table 2) are shown in Figure 4b. The sensor is embedded in a region sensitive to fibre misalignment (Flexural stress profile, Figure 4b). The tensile failure mode and load of experimental group F (Table 5) match those of the control samples, indicating successful integration of the cut ply sensors. The embedding location of the formed sensors is displayed in Figure 4b. Again, the laminate failed with a tensile failure mode, behaving in the same manner as the control samples (group G, Table 5). By separating the highly loaded plies from the sensor and using the sensor's flat underside (Figure 4b), the fibre misalignment induced in the load bearing plies was reduced, and the formed sensor integrated without reducing structural performance. To aid with the interpretation of these experimental results, and identify the causes of failure modes associated with the sensors, finite element analysis was carried out.

3. Numerical simulation

3.1. Finite element modelling methodology

To identify the load paths within each of the embedding techniques and aid with interpretation of the experimental results, two dimensional plane strain models of experimental groups D and E (Table 2, Figures 7a and 7b) were created in the finite element package ABAQUS 6.7-1. The plane strain models only permit two principle strains (ϵ_1 and ϵ_2), preventing out of plane displacements. The modelled regions and boundary conditions are displayed in Figures 7a and 7b (the drawings are not to scale).

The modelling parameters associated with each simulation are shown in Table 6. The idealised sensor geometries (identified using optical microscopy) shown in Figures 5c and 5d, were used to construct each of the models (Figures 7a and 7b). In the model of experimental group D (Figure 7a), the decrease in fibre waviness with increasing distance from the embedded sensor (Table 4) is not accounted for, making the model slightly conservative. The contact between the rollers and flexural specimens was modelled as frictionless, and the rollers assumed to be rigid, due to the stiffness of the rollers being much greater than that of the composite matrix. The appropriate material properties were assigned to each ply depending on their orientations (Hexcel E-Glass 913 prepreg, Hexcel materials data sheet). Classical laminate theory [22] was used to calculate an equivalent set of material properties to model the $\pm 45°$ layers. The mesh of each model contained locally fine regions, in locations where interlaminar stress concentrations existed (shown as horizontal and vertical lines drawn onto Figures 7a and 7b). The mesh density of each model was increased until the force applied by the loading pin converged to four significant figures for an applied displacement of 5 mm, resulting in meshes with the parameters shown in Table 6.
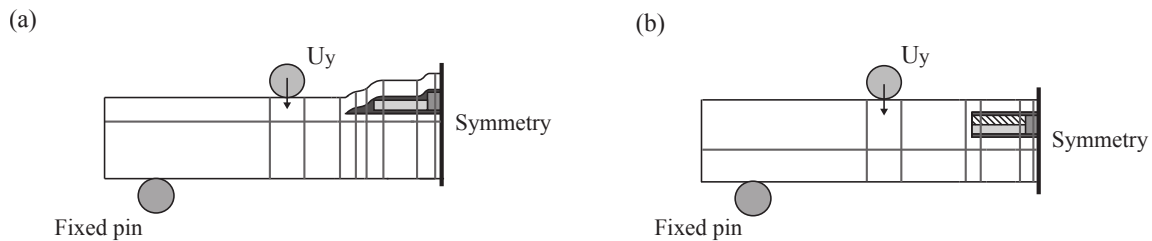

Figure 7. a) Modelled region of experimental group D (Table 2). b) Modelled region of experimental group E (Table 2). In each figure regions of high local mesh density are indicated by the horizontal and vertical lines drawn onto the specimen cross sections. The figures are not drawn to scale.

Table 6. Parameters associated with each of the models.

Global element width (mm)	Local element width (mm)	Uy - Applied displacement (mm)	Element type
0.1	0.025	5	CPE8R

3.2. Finite element results

The simulated and experimentally observed load deflection gradients of the flexural specimens (groups D and E, Table 2) are shown in Table 7 (Linear region of the experimental load deflection data). The values for each of the models are in good agreement with the experimental results, indicating that the simulations (Figures 7a and 7b) are representative of the flexural strength testing. A number of authors have shown that embedding items within composite materials results in the generation of

Table 7. Experimental and simulated, force extension gradients of the flexural specimens.

Experimental Group	Experimental (N/mm)	Simulated (N/mm)
D	130 ± 11	138
E	120 ± 9	125
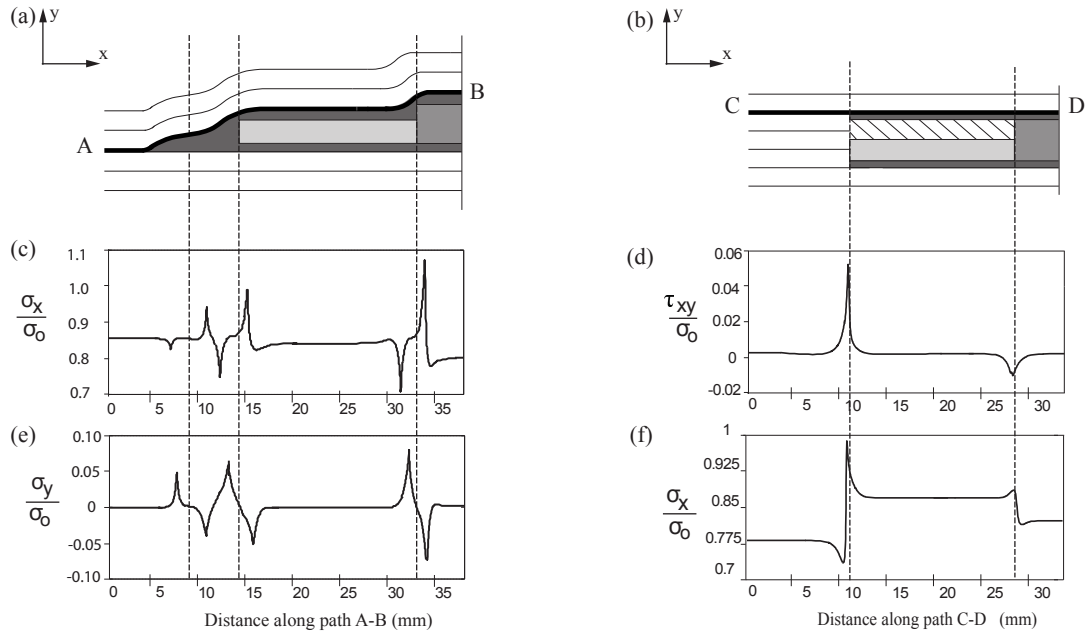
Figure 8. a) Detailed view of the formed sensor in Figure 7a. b) Detailed view of the cut ply sensor in Figure 7b. c) Axial stress along the path A-B. d) Interlaminar shear stress along the path C-D. e) Transverse stress along the path A-B. f) Axial stress along the path along the path C-D. The plotted stress values were normalised by the nominal compressive flexural stress applied to the beams.

interlaminar stresses [6, 10, 11, 13]. The finite element results in this section (Figures 8a and 8b), identify the interlaminar stress concentrations created by embedding the inductively coupled sensors within the flexural strength specimens, aiding with the interpretation of the results of the flexural strength testing (Table 5).

A detailed diagram of the formed sensor embedded in specimen group D (Tables 2 and 5), is shown in Figure 8a. The axial stress along the path A-B (Figure 8a) is plotted in Figure 8c. The simulation identified the region of plies directly above the transducer-coil interface as being the most likely to fail in compression (Largest compressive stress concentration, Figure 8c), at the region of maximum fibre misalignment (Table 4 and Figure 5d), which corresponded to the location of compressive failure in group D (Table 5 and Figure 6c). At each stepped change in sensor thickness the plies above are offset, this offsetting puts the plies into bending, and leads to the development of transverse stresses (Plotted in Figure 8e) at each change in sensor thickness. Similar behaviour is responsible for the generation of transverse stresses in tapered laminates [27]. The

maximum transverse tensile stresses exist above the transducer (Maximum change in sensor thickness and misalignment angle, Table 4). The finite element results are supported by the observed failure mode of experimental group C (Disbonding failure between transducer and bond ply, Table 5 and Figures 6b). The results indicate that when embedding sensors using the forming technique, both axial and transverse tensile stress concentrations are generated. To embed a formed sensor into composites successfully, the sensor should be embedded away from the highly loaded plies so that the misalignment introduced into the major load bearing plies is minimised. The effect of sensor integration could be further reduced by moulding the sensor prior to embedding, with a constant shallow taper angle. This would reduce both the axial and transverse stress concentrations produced by the offset plies, which are controlled by the taper angle [27, 28].

The cut ply sensor embedded in specimen group E (Tables 2 and 5), is shown in Figure 8b. The shear stress along the path C-D (Figure 8a) is plotted in Figure 8d. A large shear stress concentration exists at the ply cut, which is in agreement with other models of cut plies in tapered and unidirectional laminate specimens [29, 30]. A second smaller shear stress concentration exists above the transducer. The direction of these shear stresses are of the opposite sign; the shear stresses transfer bending load to the transducer. The axial stress along the path C-D, is plotted in Figure 8f. At each shear stress concentration there is a change in the bending load carried by the ply above the sensor. The model shows that load is transferred by shear stresses in a laminate containing a sensor embedded using the cut ply method. The magnitude of the shear stress concentration at the ply cut is determined by the amount of load carried by the cut plies. Therefore, when embedding using the cut ply method, a sensor should only be embedded in an unloaded region of the composite structure.

4. Conclusion

This work shows that high aspect ratio sensors can be embedded within composite materials, without significantly reducing structural performance. Interlaminar shear strength testing identified an encapsulating layer that provided strong adhesion between the embedded sensors and surrounding composite matrix. The increased adhesion between the sensors and surrounding material prevented the sensors acting as sites for delamination initiation.

Flexural strength testing demonstrated two techniques capable of embedding sensors without reducing flexural performance (termed the forming, and cut ply embedding methods). The forming technique was shown to embed sensors without compromising structural performance, providing the sensors through-thickness embedding location was selected so as to minimise the fibre misalignment induced in the adjacent highly loaded plies. The cut ply method, in which some of the non-load bearing plies of the laminate were cut, and the sensor inserted with a thickness that matched that of the removed plies, resulted in a less detrimental effect on the structural performance of the flexural

specimens.

This paper outlines the possible solutions for designing and embedding remote sensors (devices that do not directly interact with the sensed damage) within composite materials. The results provide a guideline for structural engineers wishing to embed sensors inside structural composite components.

Acknowledgments

5. References

[1] K Diamanti and C Soutis. Structural health monitoring techniques for aircraft composite structures. *Progress in Aerospace Sciences*, 46(8):342–352, 2010.

[2] J W C Pang and I P Bond. A hollow fibre reinforced polymer composite encompassing self-healing and enhanced damage visibility. *Composites Science and Technology*, 65(11):1791–1799, 2005.

[3] S Mall. Integrity of graphite/epoxy laminate embedded with piezoelectric sensor/actuator under monotonic and fatigue loads. *Smart Materials and Structures*, 11(4):527–533, 2002.

[4] S Mall and J M Coleman. Monotonic and fatigue loading behavior of quasi-isotropic graphite/epoxy laminate embedded with piezoelectric sensor. *Smart Materials and Structures*, 7(6):822–832, 1998.

[5] J C Fish and A J Vizzini. Tailoring concepts for improved structural performance of rotorcraft flexbeams. *Composites Engineering*, 2(5):303–312, 1992.

[6] D A Singh and A J Vizzini. Structural integrity of composite laminates with interlaced actuators. *Smart Materials and Structures*, 3(1):71–79, 1994.

[7] D R Shukla and A J Vizzini. Interlacing for improved performance of laminates with embedded devices. *Smart materials and structures*, 5(2):225–229, 1996.

[8] J P Hansen and A J Vizzini. Fatigue response of a host structure with interlaced embedded devices. *Journal of Intelligent Material Systems and Structures*, 11(11):902–909, November 2000.

[9] F Ghezzo, Y Huang, and S Nemat-Nasser. Onset of resin micro-cracks in unidirectional glass fiber laminates with integrated SHM sensors: Experimental results. *Structural Health Monitoring*, 8(6):477–491, June 2009.

[10] Y Huang, F Ghezzo, and S Nemat-Nasser. Onset of resin micro-cracks in unidirectional glass fiber laminates with integrated SHM sensors: Numerical analysis. *Structural Health Monitoring*, 8(6):493–507, August 2009.

[11] C-Y Huang, R S Trask, and I P Bond. Characterization and analysis of carbon fibre-reinforced polymer composite laminates with embedded circular vasculature. *Journal of the Royal Society, Interface / the Royal Society*, 7(49):1229–41, August 2010.

[12] K Shivakumar and L Emmanwori. Mechanics of failure of composite laminates with an embedded fiber optic sensor. *Journal of Composite Materials*, 38(8):669–680, April 2004.

[13] K Shivakumar and A Bhargava. Failure mechanics of a composite laminate embedded with a fiber optic sensor. *Journal of composite materials*, 39(9):777–798, 2005.

[14] M Lin and F-K Chang. The manufacture of composite structures with a built-in network of piezoceramics. *Composites Science and Technology*, 62(7):919–939, 2002.

[15] X P Qing, S J Beard, A Kumar, T K Ooi, and F-K Chang. Built-in sensor network for structural health monitoring of composite structure. *Journal of Intelligent Material Systems and Structures*, 18(1):39–49, October 2006.

[16] C H Zhong, A J Croxford, and P D Wilcox. Investigation of inductively coupled ultrasonic transducer system for NDE. *IEEE Transactions on Ultrasonics, Ferroelectrics and Frequency Control*, 60(6):1115–1125, June 2013.

[17] C H Zhong, A J Croxford, and P D Wilcox. Remote inspection system for impact damage in large composite structure. *Proceedings of the Royal Society of London A: Mathematical, Physical and Engineering Sciences*, 471(2173), 2014.

[18] H-Y Tang, C Winkelmann, W Lestari, and V La Saponara. Composite structural health monitoring through use of embedded pzt sensors. *Journal of Intelligent Material Systems and Structures*, 22(8):739–755, May 2011.

[19] M Yasaee. Interlaminar crack arrest in composites. *PhD Thesis, University of Bristol*, 2012.

[20] BS EN 2563:1997. British standard aerospace series, carbon fibre reinforced plastics- unidirectional laminates determination of apparent interlaminar shear strength. 1997.

[21] ASTM D6272 10. Standard test method for flexural properties of unreinforced and reinforced plastics and electrical insulating materials by four-point bending. 2010.

[22] R F Gibson. *Principles of Composite Material Mechanics*. CRC Press Taylor & Francis Group, Boca Raton, 2nd edition, 2007.

[23] M R Wisnom and J W Atkinson. Reduction in tensile and flexural strength of unidirectional glass fibre-epoxy with increasing specimen size. *Composite Structures*, 38(1):405–411, 1997.

[24] R S Trask and I P Bond. Biomimetic self-healing of advanced composite structures using hollow glass fibres. *Smart Materials and Structures*, 15(3):704–710, June 2006.

[25] M J Pavier and M P Clarke. Finite element prediction of the post-impact compressive strength of fibre composites. 36(1996):141–153, 1997.

[26] Z Aslan and M Şahin. Buckling behavior and compressive failure of composite laminates containing multiple large delaminations. *Composite Structures*, 89(3):382–390, July 2009.

[27] D-J Shim and P A Lagace. Mechanisms and structural parameters affecting the interlaminar stress field in laminates with ply drop-offs. *Journal of composite materials*, 40(4):345–369, 2006.

[28] C A Steeves and N A Fleck. Compressive strength of composite laminates with terminated internal plies. *Composites Part A: applied science and manufacturing*, 36(6):798–805, 2005.

[29] W Cui, M R Wisnom, and M Jones. Effect of step spacing on delamination of tapered laminates. *Composites Science and Technology*, 52(1):39–46, January 1994.

[30] W Cui, M R Wisnom, and M Jones. An experimental and analytical study of delamination of unidirectional specimens with cut central plies. *Journal of Reinforced Plastics and Composites*, 13(8):722–739, 1994.